Biradical states of oxygen-vacancy defects in α-quartz

R. I. Mashkovtsev*
Institute of Geology and Mineralogy, SB RAS, 630090 Novosibirsk, Russia

D. F. Howarth and J. A. Weil†
Department of Chemistry, University of Saskatchewan, Saskatoon, Saskatchewan, Canada S7N 5C9
(Received 31 July 2007; revised manuscript received 16 October 2007; published 21 December 2007)

Several radiation defects with effective electron spin $S=1$ have been observed in synthetic α-quartz, using room-temperature (RT) electron paramagnetic resonance (EPR) spectroscopy. It turns out that these defects had better be considered as biradicals, i.e., pairs of $S=1/2$ species. The parameter matrices $\mathbf{g}_1$, $\mathbf{g}_2$, $\mathbf{D}$ as well as matrices $\mathbf{A}$ describing the hyperfine interactions with two slightly inequivalent ^{29}Si nuclei have been determined for the most intense (but RT unstable) such defect, which herein is labeled E_1''. The triplet-state approach and the biradical approach are compared. Inter-electron distances have been estimated using magnetic dipole concepts. A structure for center E_1'' is proposed, suggesting an oxygen (O^0) vacancy with two unpaired electrons (holes) existing at silicon cations on opposite sides of the cavity, and the model is compared with the observed data and with published results for related single-unpaired electron species. Firm correlations between spin-Hamiltonian parameter matrix principal axes (EPR data) and crystallographic directions (x-ray diffraction data) have been attained.

DOI: 10.1103/PhysRevB.76.214114 PACS number(s): 61.72.Hh, 76.30.Mi, 42.70.Ce

I. INTRODUCTION

Silicon dioxide in its various forms is among the most extensively used materials. Since many of its interesting properties persist in its different varieties, SiO_2 is used in many forms and for various purposes. The importance of oxygen-deficient defects in SiO_2 arises mostly from the wide application of the material in a variety of electronic and optical devices. In all of these applications, the nature and number of defects are crucial to the reliability. On the more esoteric side, SiO_2 is the material which recently has permitted the first single electron spin detection.[1]

The pointlike centers in α-quartz have been studied extensively over the past 50 years, both experimentally and theoretically (for reviews, see Refs. 2–5). For instance, the detailed analysis of a biradical center in α-quartz investigated by electron paramagnetic resonance (EPR) spectroscopy has been published, but is not yet well understood.[6] The well-known paramagnetic E' defects, each with a single unpaired electron (spin $S=1/2$), and thought to be associated with an oxygen vacancy, are quite abundant and can be easily generated in SiO_2.

Experimental results for center E_1' (Refs. 7–9) have caused lengthy discussions about the model of this center. The substantial spin density observed in one Si sp^3 nonbonding orbital is not in accord with the presence of a single oxygen vacancy. An agreement with the experimental result is possible provided a sufficiently large asymmetric relaxation of the two Si atoms facing the vacancy is involved. In α-quartz, the asymmetry for a positively charged oxygen vacancy, $V(O)^+$, was originally proposed by Feigl *et al.*[10] in 1974. Further theoretical efforts have improved this assumption.[11–13] The positive charge state yields a minimum-energy configuration with large relaxation of the silicon Si1 (Fig. 1) on the long-bond side of the vacancy. This silicon is thought to move through its basal oxygen plane and to bond with an oxygen atom, making that O atom threefold coordinated, and the spin is localized on the other silicon Si0, moved toward the oxygen vacancy [e.g., O(I) in Fig. 1]. In 1997, Boero *et al.*[14] offered an accurate theoretical estimate of the ^{29}Si hyperfine (HF) coupling parameters for E_1' in α-quartz and the equivalent center E_γ' in vitreous silica (a-quartz), one that turns out to be in rather good agreement with the experimental result,[9] and thus, a general consensus about a microscopic model has nearly been reached. However, alternative models have been proposed, involving a

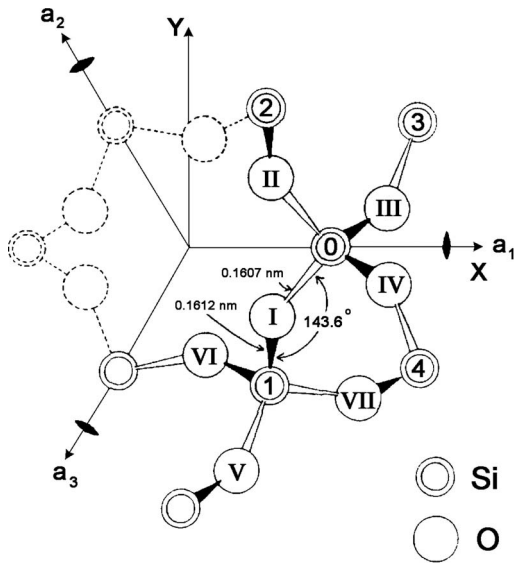

FIG. 1. Portrait of a fragment of the crystalline structure of α-quartz showing a Si_2O_7 unit including the neighboring silicon atoms (see Ref. 19). Here, the three axes a_i are the piezoelectric axes, and axis **z** (not shown, $\perp$ plane of the paper, at the origin) is the crystal optic axis **c**. The oxygen anions are labeled with Roman numerals.

bridged hole-trapping oxygen-deficiency center[15] or different types of puckered configuration[16] in amorphous quartz: a-SiO_2. The positive charged state $V(O)^+$ was found to be unstable in α-quartz with respect to the solid-state reaction $2V(O)^+ \rightarrow V(O)^0 + V(O)^{2+}$, and it was proposed that $V(SiO_3)^+$ or $V(SiO_4)^+$ are the smallest possible EPR-active vacancy complexes.[17] Recently, via a first-principles molecular-dynamics study, it was suggested to characterize E' centers as featuring merely a (modest) displacement of an O atom in a ≡Si—O—Si≡ unit *without* removing the atom from the crystal system.[5,18]

Among the best-known $V(O)$ centers (E_1', E_2', and E_4'), E_4' contains atomic hydrogen bonded to one of the Si atoms and is thought to have the form $[O_3Si0:H\cdot Si1O_3]^0$ (designation corresponds to Fig. 1),[19] and this configuration was supported by further theoretical work.[20–22] Another paramagnetic center, E_2', also exhibits a proton HF structure attributed to hydrogen, but is more poorly understood. From the EPR method, it was deduced that, here, the unpaired spin is localized in an sp^3 orbital pointing toward the oxygen-substituted hydrogen along a long-bond direction[23] and, from molecular-orbital calculation, center E_2' was proposed to be a variant of E_4' with a back-projected dangling-bond configuration.[24] Recently, further EPR work on the various E' centers has been completed, including a description of a second type of E_2' center.[25]

Experimental and theoretical investigations on any neutral oxygen vacancy in its multi-unpaired-electron state might well provide a deeper insight into the general problem. Yet, for α-quartz, the experimental work has remained in a very incomplete state since 1965, and the needed principal values and directions of the spin-Hamiltonian parameter matrices have not materialized.[26–28]

There are a few works[29,30] on amorphous SiO_2 where a "triplet" center was detected but, in noncrystalline material, the EPR method has not given adequately complete information about the structure of the observed defects. As reported some years ago,[31] and more recently,[29] a weakly allowed transition at $g \sim 4$ (and no other) was observed. In earlier work, a "biradical" center in a-silica with $g=2.002$ and $D/(g_e\beta_e)=13.4$ mT was related to an oxygen-vacancy defect, probably "decorated" with Cl^- ions (no HF splitting from these were seen), but was incompletely described.[30] In general, a sparse experimental background, if used for theoretical calculations,[32,33] could well lead to inappropriate results.

We have observed six other radiation-induced centers, each initially thought to occur in a spin triplet state. Among them were three centers already briefly described in several papers.[26–28] It now has turned out that these centers had better be regarded as biradical centers (Refs. 6 and 34, Sec. 6.5). We can take advantage of the narrow EPR lines we encounter (allowing accurate line-position measurement), and the single-crystal observed anisotropy of the spectra, to measure and present accurate spin-Hamiltonian parameters, and we can now propose a model for the most intense such center, designated herein as E_1''.

II. QUARTZ CRYSTAL STRUCTURE

The crystals used in our work were right-hand α-quartz. We use the crystal coordinate system consisting of a right-handed Cartesian axis set, in which the z axis is the c (optic) axis and the x axis is parallel to (any) one a_1 of the three piezoelectric axes (see Fig. 1). The positive end of the x axis develops a negative charge on compression along x. The polar angle θ is measured from the positive z axis (arbitrary choice), and the azimuthal angle φ from the positive x axis.

TABLE I. Structure of any Si_2O_7 unit in perfect α-quartz at 94 K, as shown in Fig. 1 (wherein oxygens are labeled with Roman numbers), calculated from the 94 K crystal structure data of Ref. 35.

Atoms	Cartesian coordinates (nm) of atoms		
	x	y	z
Si0	0.23094	0	0
Si1	0.13031	−0.22571	−0.18021
O1	0.13758	−0.11396	−0.06423
O2	0.13758	0.11396	0.06423
O3	0.32409	0.06217	−0.11598
O4	0.32409	−0.06217	0.11598
O5	0.0783	−0.36355	−0.11598
O6	0.0299	−0.17613	−0.29619
O7	0.27569	−0.24959	−0.24443

Bond	Bond lengths (nm)	Bond directions (deg)	
		θ, φ	θ, φ
Si0—O1	0.16071	66.4, 50.7	113.6, 230.7
Si1—O1	0.16122	44.0, 86.3	136.0, 266.3
Si0—Si1 [a]	0.30585	53.9, 66.0	126.1, 246.0
O1—O2	0.26163	60.6, 90	119.4, 270
O1—O3	0.26170	101.4, 43.4	78.6, 223.4
O1—O4	0.26447	133.0, 15.5	47.0, 195.5
O2—O3	0.26441	47.0, 164.5	133.0, 344.5
O2—O4	0.26170	78.6, 136.6	101.4, 316.6
O3—O4	0.26318	28.2, 270	151.8, 90

Bonds	Bond angle (deg)
O1—Si0—O2	108.974
O1—Si0—O3	108.762
O3—Si0—O4	109.415
Si0—O1—Si1	143.630

[a] We discuss the complete set of Si-O-Si directions in the text.

There are two kinds of Si—O bonds in α-quartz (Table I), labeled "long" bond (0.1612 nm) and "short" bond (0.1607 nm), as measured at 94 K.[35] Each SiO_4 unit, which has C_2 local symmetry, is close to but deviates from having a perfect tetrahedral structure. Ignoring translation operations and defects as well as surface proximity, the SiO_4 units can be said to be distributed according to symmetry group D_3 and occur in any one of three symmetry-related orientations. Each Si-O-Si unit occurs in six symmetry-related orientations.

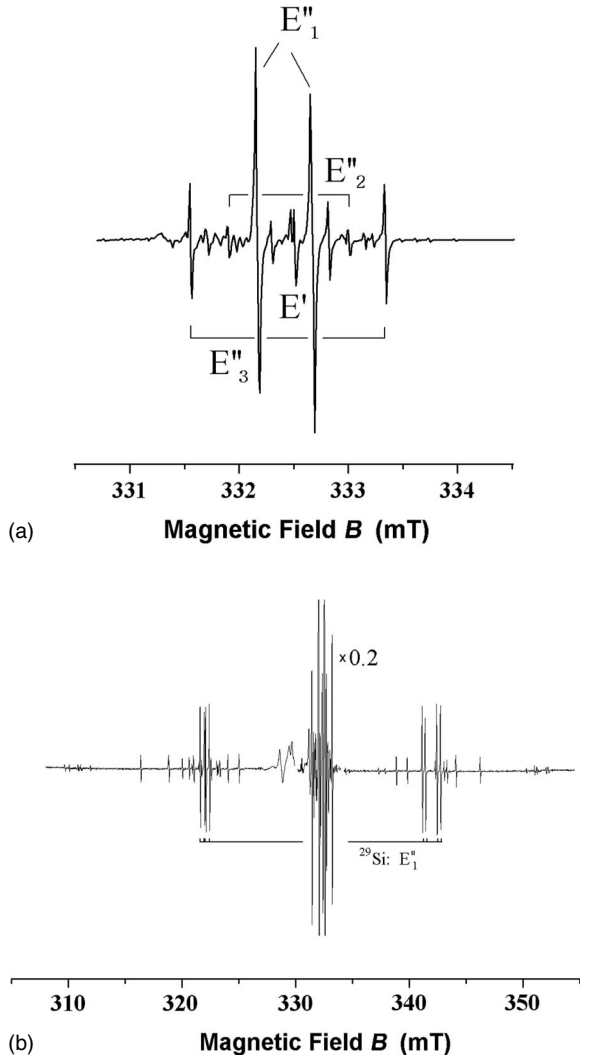

FIG. 2. Field-swept EPR spectra, taken at 9.31 GHz, for synthetic α-quartz at 293 K previously subjected to irradiation by fast electrons. The EPR measurements began within a few hours after the irradiation, with the crystal aligned $\mathbf{c}\,(=\mathbf{z}) \parallel \mathbf{B}$. (a) Central region of the spectrum showing the main lines of centers E_1'', E_2'', and E_3''. (b) Full spectrum with the substantial ^{29}Si HF splitting indicated for the center E_1''.

Any single Si_2O_7 group within the crystal consists of two SiO_4 units which share an oxygen, herein labeled O1 (Fig. 1). The latter is the anion removed when an oxygen vacancy is to be considered. In the figure, Si0-O1 is a short bond and Si1-O1 is a long bond. The Cartesian coordinates of the Si_2O_7 unit defined to contain O1 are listed in Table I, along with the directions to be compared with the principal directions of spin-Hamiltonian matrices to be presented. We find the directions of the Si-O-Si units to be important.

In modeling the various paramagnetic centers encountered here, the orientations of the entities having the smallest silicon-silicon (Si-O-Si) distance (0.30573 nm at 94 K) occurring in α-quartz evidently are important. One way to describe the situation is as follows. There are two sets of six such lines occurring in the structure, labeled A and B here. Relative to the optic axis c (z) and the piezoelectric axis a_1 ($\equiv$polar axis x), they all occur with the same polar angle,

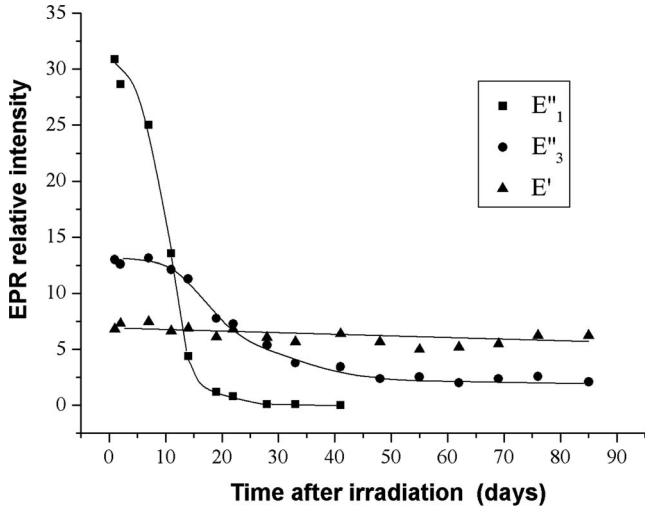

FIG. 3. EPR signal intensity as f(time) of E_1'', E_3'', and an E'-type center (g_c=2.0007) during storage at room temperature after electron irradiation.

$^0\theta = 54.0°$ (notice that both $^0\theta$ and $^0\phi$ are very close to the pure tetrahedral angle $\arccos[(1/3)^{1/2}]$), at azimuthal angles:

$$\varphi_A = {}^0\varphi + 60.0\,^\circ\, p_A$$

$$\varphi_B = 120\,^\circ - {}^0\varphi + 60.0\,^\circ\, p_B,$$

where $^0\phi = 54.0°$, and where integers p_A and p_B have the range 0–5.

For example, at tetrahedron Si(0) in Fig. 1, the inter-Si lines for Si(0)-O-Si(j) occur as j=1, p_B=0, j=2, p_A=1, j=3, p_A=3, and j=4, p_B=4. For a principal axis $^0\theta$, p_B=0 of any spin-Hamiltonian parameter matrix, the operations of group D_3 relevant to α-quartz yield five other symmetry-related lines: p_A=0,1,5 and p_B=1,5.

III. EXPERIMENTAL DETAILS

Lumbered bars of pure synthetic right-hand quartz crystals were obtained from VNIISIMS (Russia). Samples with typical dimensions of $3\times6.5\times7$ mm^3 in the X, Y, and Z directions, respectively, were cut from these bars for EPR investigations at room temperature. For low-temperature measurements, the sample dimensions were about $2\times3\times6$ mm^3.

The paramagnetic centers were induced in two ways:

(1) One sample had been irradiated (about 30 years, ago) with fast neutrons at a fluence of 5×10^{17} cm^{-2}, which heats the crystal (about 500 K), destroying various (e.g., E'') EPR centers. Hence, to produce multi-unpaired-electron centers, this sample was irradiated at 77 K with γ rays (^{60}Co source), applying a dose of about 2 Mrad. For the latter irradiation, the sample was held in a glass Dewar filled with liquid nitrogen. Furthermore, the sample was transferred to an EPR spectrometer without warming, and was then investigated at 77 K.

(2) Quite recently, to induce triplet centers, another sample was irradiated with fast electrons (3.5 MeV, dose

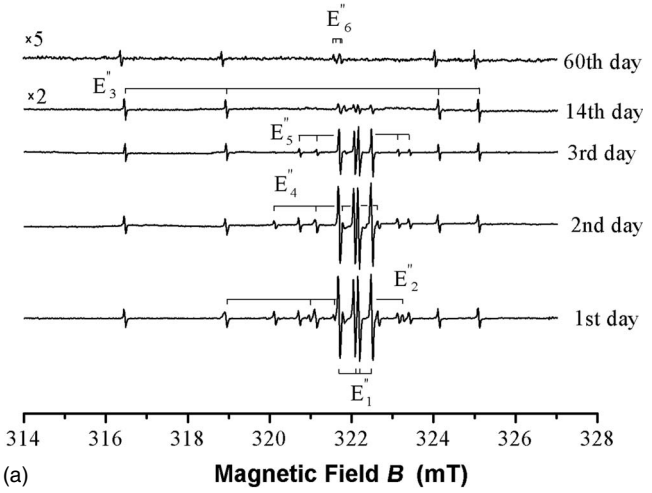

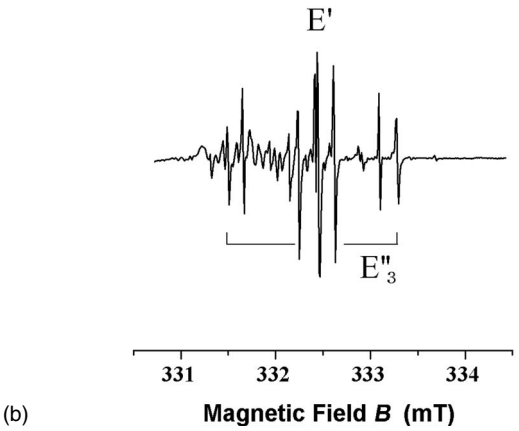

FIG. 4. EPR spectra taken with $\mathbf{B} \parallel \mathbf{c}$ at 9.31 GHz and 293 K. (a) Transformation as f(time) in the low-field region of the ^{29}Si HF splitting of the triplet centers. (b) Central region of the spectrum on the 60th day after electron irradiation. In comparison to Fig. 2(a), the ordinate scale here is increased by a factor of 2.

10^{17} cm^{-2}); here, the sample was maintained at room temperature by the cooling water flowing through the sample holder. EPR spectra were taken right away, since many signals from observable triplet centers faded at room temperature. Herein, we present mainly the results of the latter investigation.

The experimental EPR data were taken by one of the authors (R.I.M.). The EPR spectrometer used was a Radiopan SE/X 2543 (operating frequency of about 9.3 GHz) with a built-in NMR magnetometer. The sample was fastened on a homebuilt goniometer which allowed a rotation of the crystal in the cavity around two orthogonal axes. A DPPH (free radical 2,2′-diphenyl-1–picrylhydrazyl) powder reference (almost isotropic, $g=2.0037$, and linewidth $\Delta B_{\mathrm{ms}} \sim 0.1$ mT) was used to calculate the microwave frequency.

IV. EXPERIMENTAL RESULTS

Before irradiation with fast electrons, no EPR signal was observable at room temperature. Straight away after electron irradiation, a rich EPR spectrum was observed, complex even at the canonical orientation $\mathbf{B} \parallel \mathbf{c}$ (see Fig. 2).

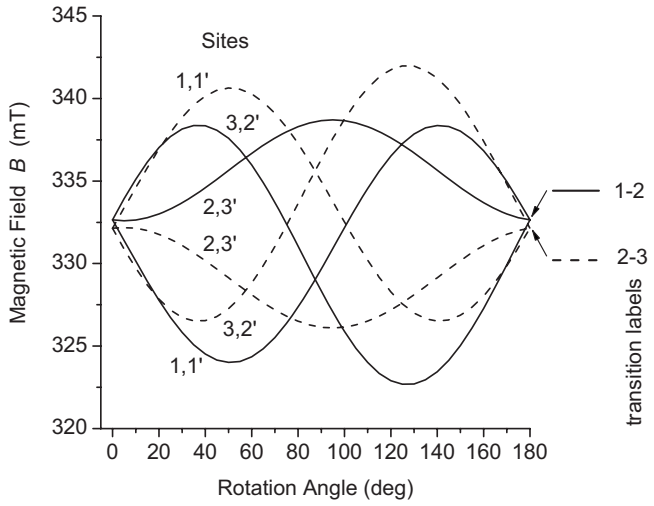

FIG. 5. Angular variation of the experimental EPR line positions for center E_1''. Primary lines as $f(B)$ at a frequency of about 9.31 GHz for rotations of $\mathbf{B}$ in the crystal plane yz. Here, z ($\theta=0$) denotes $\mathbf{B} \parallel \mathbf{c}$. The transitions are labeled consistent with the use of the triplet-state model (denoted by I herein).

A. *c*-axis electron paramagnetic resonance spectra of all paramagnetic species

In the α-quartz structure, paramagnetic centers with either C_1 or C_2 local symmetry are observed. For each C_1-symmetry center, there are six magnetically distinguishable crystal sites in any general direction of the externally applied magnetic field $\mathbf{B}$. The multi-unpaired-electron cen-

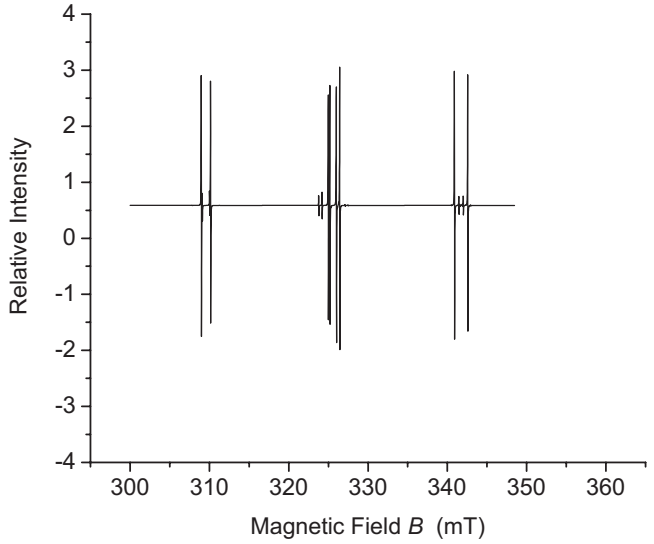

FIG. 6. Computer-simulated EPR spectrum (9.3 GHz, with $\mathbf{B} \parallel \mathbf{c}$) showing the expected spectrum for center E_1'' (triplet model) when containing both $^{29}\mathrm{Si}_\alpha$ and $^{29}\mathrm{Si}_\beta$ ($\mathbf{g}$, $\mathbf{D}$, and $\mathbf{A}$ matrices in Tables II and III). The spectrum in first-derivative presentation with Lorentzian line shapes (width of 0.03 mT) was generated using FORTRAN program EPR-NMR (Ref. 38).

TABLE II. Triplet-state analysis. Main lines: Best-fit spin-Hamiltonian parameter matrices for center E_1'' in α-quartz at about 300 K. EPR: $\nu \sim 9.3$ GHz. The matrix set below is for one crystal site, called 1. There are five other sets related by symmetry to it via the group D_3 operator matrices. The line-position difference (and frequency) data were minimized using our in-house computer program EPR-NMR (Ref. 38). Matrices **g** and **D** were evaluated by line-position difference minimization of 198 non-zero-weighted data points (about 66 for each of three sites). Sum of weighting factors=189.63, RMSD=0.0167 mT. In this table, and subsequent ones, the numbers within parentheses indicate the estimated uncertainties in the preceding numbers.

	Matrix **Y**			k	Principal values Y_k	Principal directions [a] θ_k (deg), φ_k (deg)	θ_k (deg), φ_k (deg)
$^{I}\mathbf{g}$	2.00095(2)	0.00022(2)	0.00024(1)	1	2.00156(2)	61.1(7), 58.0(1)	118.9(7), 238.0(13)
		2.00118(2)	0.00037(1)	2	2.00081(2)	91.1(26), 47.4(16)	88.9(26), 327.4(16)
			2.00076(1)	3	2.00052(2)	151.1(7), 55.4(57)	28.9(7), 235.4(57)
$^{I}\mathbf{D}/(g_e\beta_e)$ (mT)	−1.596(2)	3.938(2)	3.095(2)	1	8.126(2)	56.05(1), 56.5(1)	123.95(1), 236.5(1)
		1.766(2)	4.649(2)	2	−3.928(2)	145.87(3), 63.2(6)	34.13(3), 243.2(6)
			−0.170(1)	3	−4.198(2)	86.91(29), 148.6(2)	93.09(29), 328.6(2)

[a] The sets (θ, φ) and $(180° - \theta, 180° + \varphi)$ are equivalent.

ters behave in this fashion. For all centers, in the c-axis spectrum ($\mathbf{B} \| \mathbf{c}$), the six sites are magnetically equivalent and, thus, give superimposed EPR spectra.

In Fig. 2(a), centers E_1'', E_2'', and E_3'' [which have doublets centered at $g_c=2.0012$, 2.0010, and 2.0010, respectively, with line-pair spacings [about $3|D_{zz}|/(g_e\beta_e)$ of 0.51, 1.10, 1.79 mT] are shown. In the middle of the spectrum, E'-type centers are also observable (single lines at $g_c=2.0007$ and two lines near $g_c=2.0008$, separated by 0.04 mT). The max-to-min first derivative (max slope points of the absorption) width ΔB_{ms} of the individual EPR line is about 0.03 mT. The temporal behavior of some of these centers is indicated in Figs. 3 and 4. Furthermore, for the triplet centers, half-field $\Delta M_S = \pm 2$ transitions were observed. The various lines are easily saturated with microwave power applied at room temperature. In some cases, in our measurements, the primary lines were slightly broadened due to slightly too high field modulation.

Also, many lines from other centers are observed. For example, in the central region of the spectrum, there is a doublet (with $g_c=2.0008$ and splitting 0.38 mT) arising from an unknown center, and two doublets ($g_c=2.0012$ with splittings 0.49 and 1.44 mT) arising from the E_4' center [visible in Fig. 4(b), but partly veiled].

Also, a large number of pairs of HF lines from ^{29}Si nuclei ($I=1/2$, natural abundance of 4.69 at. %) are observed [see Fig. 2(b)] in the field range of the E'-type centers. The HF splittings are about 40 mT. Also, there are HF quartets in the range of the triplet centers E'' (with splittings of about 20 mT). We have confirmed, by measuring the intensities relative to the much more intense primary lines, that these pairs and quartets are ^{29}Si HF structures in the EPR spectrum

TABLE III. $^{29}\mathrm{Si}_\alpha$ and $^{29}\mathrm{Si}_\beta$ hyperfine matrices, derived from model I. Best-fit spin-Hamiltonian parameter matrices for center E_1'' in α-quartz at about 300 K. EPR: $\nu \sim 9.3$ GHz. The matrix sets below are for one crystal site, called 1. There are five other sets related by symmetry to them via the group D_3 operator matrices. The line-position difference (and frequency) data were minimized using our in-house computer program EPR-NMR (Ref. 38).

	Matrix **Y**			k	Principal values Y_k	Principal directions [a] θ_k (deg), φ_k (deg)	θ_k (deg), φ_k (deg)
$^{I}\mathbf{A}(^{29}\mathrm{Si}_\alpha)/(g_e\beta_e)$ (mT) [b]	21.176(9)	1.148(8)	1.075(7)	1	22.65(1)	62.1(1), 34.2(1)	117.9(1), 214.2(1)
		20.257(9)	0.748(7)	2	19.49(1)	53(10), 148(9)	127(10), 328(9)
			20.171(5)	3	19.46(1)	130(10), 98(10)	50(10), 278(10)
$^{I}\mathbf{A}(^{29}\mathrm{Si}_\beta)/(g_e\beta_e)$ (mT) [c]	18.780(8)	0.251(6)	0.134(5)	1	21.994(7)	61.1(1), 84.2(1)	118.9(1), 264.2(1)
		21.217(7)	1.358(5)	2	18.768(6)	147(10), 53(34)	33(10), 233(34)
			19.518(4)	3	18.753(7)	104(18), 166(11)	76(18), 346(11)

[a] The sets (θ, φ) and $(180° - \theta, 180° + \varphi)$ are equivalent.

[b] Matrix $^{I}\mathbf{A}[^{29}\mathrm{Si}_\alpha]$ was evaluated using 414 non-zero-weighted data points (about 140 for each of three sites). Sum of weighting factors = 414 and RMSD = 0.0341 mT.

[c] Matrix $^{I}\mathbf{A}[^{29}\mathrm{Si}_\beta]$ was evaluated using 414 non-zero-weighted data points (about 140 for each of three sites). Sum of weighting factors = 414 and RMSD = 0.0264 mT.

of various centers. There are, weak in intensity, five pairs of single lines and one pair of doublets ($A_c/(g_e\beta_e)=0.04$ mT) in the range of E'-type ^{29}Si HF structure with calculated $g_c=2.0007\pm0.0005$ and splittings of 38.3, 39.9, 40.29, 40.45, 41.95, and 42.54 mT, respectively. Single lines and doublets with splitting $A_c/(g_e\beta_e)=40.45$ and 42.54 mT correspond to ^{29}Si HF structure of centers E_1' and E_2', respectively.[8,23,27] Also, we note that at some orientations, for center E_1'', additional small doublets appear to be present, centered on and outside the ^{29}Si lines, with isotropic splitting of about 0.05 mT; this line set was not detectable at $\mathbf{B}\parallel\mathbf{c}$, perhaps due to many of the lines superimposed within the relevant B region.

All the triplet centers observed by us are unstable at room temperature. The center E_2'' was not visible on the day after irradiation. The temporal stability of two such centers in comparison to that of the E'-type center is shown in Fig. 3. Center E_1'' was no longer observable after about 40 days, while E_3'' was still visible after 100 days of (RT) storage. In Fig. 4(a), the transformation of the ^{29}Si HF region in the lower-field side of the hyperfine spectrum is demonstrated. From this figure, we deduce that possibly there are six independent patterns of ^{29}Si HF lines. Some idea of the stability with time can be gleaned from Fig. 4(b).

In addition, we now briefly describe older results obtained from a neutron-irradiated sample.[27] After this irradiation at room temperature, the pattern of paramagnetic centers with an intense E_1' enter resonance, among them (at 77 K) the well-known aluminum hole center $[AlO_4]^0$,[36] was observed. We noted that, after low-temperature γ irradiation, the signal from E_1' was greatly diminished and that its ^{29}Si HF structure could not be observed. At 77 K, three main triplet centers were observed with splitting, which were not distinguishable from ones at room-temperature measurement. With *in situ* annealing of the latter centers at 353 K, the E_1' center was not restored at once, but was observed again after annealing the sample at 393 K. Furthermore, the triplet centers were unstable under exposure to sunlight, and were effectively bleached under Hg lamp irradiation with a 313 nm filter in place.

At directions of $\mathbf{B}$ restricted to $\mathbf{B}\perp\mathbf{a}_1$, the main EPR spectrum of E_1'' consists of six lines (three lines for each of the two primary transitions allowed for electron spin $S=1$), along with two different sets of ^{29}Si HF lines [see Fig. 2(b)] with equal intensity. This fact intimates that any unpaired electron sees different surroundings when located on or near each of the two silicon cations.

No site splitting of these spectra was detected due to deviations from $\mathbf{B}\perp\mathbf{a}_1$, at any rotation angle. EPR spectra were recorded through 5° intervals when the crystal was rotated by 180° around the a_1 axis, with $\mathbf{B}\perp\mathbf{a}_1$. In this rotation, each EPR line is doubly degenerate,[37] and thus, only three sites are magnetically distinguishable. The crystal-rotation line-position curves are shown in Fig. 5, for constant microwave frequency.

B. Spin-Hamiltonian parameters of center E_1''

Using the computer program EPR-NMR,[38] the various parameter matrices $\mathbf{g}$, $\mathbf{D}$, and $\mathbf{A}$ (taken to be symmetric real) were calculated in two ways:

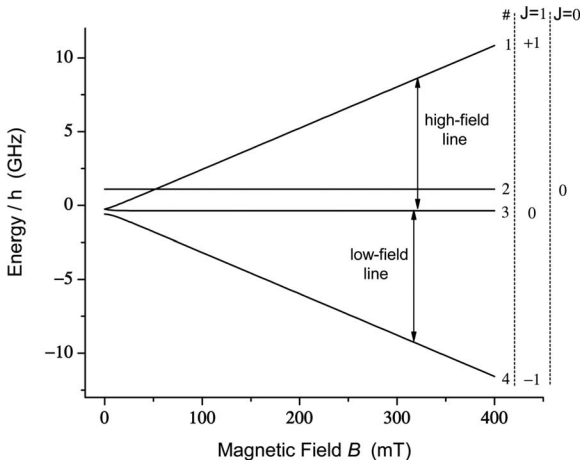

FIG. 7. Zeeman energy-level scheme for center E_1'' with $\mathbf{B}\parallel\mathbf{c}$, derived using data appropriate for the biradical model, ignoring ^{29}Si hyperfine effects. Note that the singlet state has been placed energetically just above the triplet-state energy at $B=0$, running parallel in energy to that of the $M_S=0$ level of the triplet. Thus, for this example, $J<0$.

(I) With the triplet-state spin Hamiltonian (Ref. 34, Sec. 6.8)

$$^{\mathrm{I}}\mathcal{H}=\beta_e\mathbf{B}^T\cdot\mathbf{g}\cdot\mathbf{S}+\mathbf{S}^T\cdot\mathbf{D}\cdot\mathbf{S}+\mathbf{I}_i^T\cdot\mathbf{A}_i\cdot\mathbf{S}-\beta_n\mathbf{B}^T\cdot\mathbf{g}_{ni}\cdot\mathbf{I}_i, \tag{1}$$

with primary spin quantum numbers $S=1$ and $I_i=1/2$, where $i=\alpha$ or β for two slightly inequivalent ^{29}Si nuclei present in a small (0.047) mole fraction of the centers. Thus, for most of the centers present (main EPR lines), the last two terms are absent. In the above, β_e and β_n are the electronic (Bohr) and nuclear magnetons, and the two matrices $\mathbf{g}$ are the corresponding Zeeman splitting parameter matrices. Matrix $\mathbf{D}$ has five parameters giving the electronic quadrupole energy.[34] Matrix $\mathbf{A}$ contains the six parameters describing the ^{29}Si hyperfine interaction. When needed for clarity, preceeding superscripts I or II indicating the model will be attached to the matrix symbols.

(II) With the biradical-state spin Hamiltonian (Ref. 6 and Sec. 6.5 of Ref. 34)

$$^{\mathrm{II}}\mathcal{H}=\beta_e\mathbf{B}^T\cdot(\mathbf{g}_1\cdot\mathbf{S}_1+\mathbf{g}_2\cdot\mathbf{S}_2)+[(\mathbf{S}_1{}^T\cdot\mathbf{J}\cdot\mathbf{S}_2+\mathbf{S}_2{}^T\cdot\mathbf{J}\cdot\mathbf{S}_1)/2]+\mathbf{I}_i^T\cdot\mathbf{A}_i\cdot\mathbf{S}_1+\mathbf{I}_i^T\cdot\mathbf{A}_i\cdot\mathbf{S}_2-\beta_n\mathbf{B}^T\cdot\mathbf{g}_{ni}\cdot\mathbf{I}_i. \tag{2}$$

For the latter, $S_1=S_2=1/2$. Here, matrix $\mathbf{J}\equiv J\mathbf{E}+{}^{\mathrm{II}}\mathbf{D}$, where J is the scalar exchange energy and $\mathbf{E}$ is the 3×3 unit matrix, and

$$^{\mathrm{II}}\mathbf{D}\equiv(\mathbf{g}_1{}^T\cdot{}^0\mathbf{D}\cdot\mathbf{g}_2+\mathbf{g}_2{}^T\cdot{}^0\mathbf{D}\cdot\mathbf{g}_1)/2g_e{}^2. \tag{3}$$

Each matrix $\mathbf{g}_j$ $(j=1,2)$ and $\mathbf{A}_i$ contains six independent parameters to be fitted. The electronic quadrupole matrices $^{\mathrm{I}}\mathbf{D}$ in $^{\mathrm{I}}\mathcal{H}$ and $^0\mathbf{D}$ in $^{\mathrm{II}}\mathcal{H}$ have only five since their traces are zero. In both cases, the parameters in matrices $\mathbf{g}$ and $\mathbf{D}$ were calculated to fit the primary line positions.

Perhaps we should clarify that the second right-hand term in Eq. (2) splits the energy into a singlet and a triplet spin system (Fig. 6.2 of Ref. 34). We deal with a biradical species

TABLE IV. Biradical-state analysis. Spin-Hamiltonian parameter matrices for center E_1'' in α-quartz at about 300 K. EPR: $\nu \sim 9.3$ GHz. The matrix set below is for one crystal site, called 1. There are five other sets related by symmetry to it via the group D_3 operator matrices. The line-position difference (and frequency) data were minimized using our in-house computer program EPR-NMR (Ref. 38). Matrices $\mathbf{g}_1$, $\mathbf{g}_2$, and $^0\mathbf{D}$ were evaluated by line-position difference minimization of 198 non-zero-weighted data points (about 66 for each of three sites). Sum of weighting factors=189.63 and RMSD=0.016 07 mT. Note: The uncertainties in the diagonal elements of $^0\mathbf{D}$ are ~0.3 mT.

	Matrix **Y**			k	Principal values Y_k	Principal directions θ_k (deg), φ_k (deg)	Principal directions θ_k (deg), φ_k (deg)
$\mathbf{g}_1$	2.0014(3)	0.0004(2)	−0.0002(3)	1	2.0019(3)	103(9), 47(16)	77(9), 227(16)
		2.0014(5)	−0.0004(3)	2	2.0010(2)	99(22), 139(12)	81(22), 319(12)
			2.0001(2)	3	2.0000(3)	16(13), 84(59)	164(13), 264(59)
$\mathbf{g}_2$	2.0010(5)	0.0000(3)	0.0007(3)	1	2.0025(5)	39(6), 67(18)	141(6), 247(18)
		2.0010(5)	0.0012(3)	2	2.0006(2)	99(14), 145(8)	81(14), 325(8)
			2.0014(2)	3	1.9997(1)	127(6), 48(12)	52(6), 228(12)
$^0\mathbf{D}/(g_e\beta_e)$ (mT)	−3.19	7.873(3)	6.194(3)	1	16.25	56.05(1), 56.49(1)	123.95(1), 236.49(1)
		3.53	9.301(3)	2	−7.86	145.85(4), 63.6(6)	34.2(1), 243.6(6)
			−0.34	3	−8.39	86.7(3), 148.7(2)	93.3(3), 328.7(2)
J (mT)		−4.56(8)					

when $J \sim 0$, i.e., same magnitude as k_bT (about 2.5 kJ mol^{-1} at room temp; $J/g_e\beta_e \sim 0.2$ mT). When this is not so, one deals with a triplet state: for $J \gg 0$, the triplet is high in energy compared to that of the corresponding singlet state (the latter then containing "all" the spins), whereas $J \ll 0$ implies that the singlet is high in energy and basically is unpopulated.

We note that the parameter matrices in each of the two spin Hamiltonians are for one of the (of six) symmetry-related sites, which we call site 1, chosen after noting that for it there is fine correlation with a structural Si-O-Si direction for the tetrahedron depicted (see Fig. 1) as located on axis $\mathbf{a}_1$ It is the site for which the orientation of the relevant Si-Si direction has the smallest azimuthal angle (see Sec. II).

We now consider the sign choice for the parameter matrices, i.e., multiplication by the same choice ±1 for all elements of each. The signs of matrices $\mathbf{g}$ in all cases are fixed with principal values positive. When fitting matrix $^{\mathrm{I}}\mathbf{D}$ in model I, the choice is arbitrary at this time. [Very-low-temperature EPR intensity data could contribute some knowledge of the relative energy-state populations (Ref. 34 p. 167).] Consideration of our ^{29}Si hyperfine data shows that the sign of each $\mathbf{A}$ is linked to that of $\mathbf{D}$. Thus, with model II, the relative signs of $\mathbf{A}(\mathrm{Si}_\alpha)$ and $\mathbf{A}(\mathrm{Si}_\beta)$ also are not independent. However, the signs of matrices $^0\mathbf{D}$ and of parameter J are independent. The signs of $^0\mathbf{D}$ and ^{29}Si matrices $\mathbf{A}$ are linked, as is so for $^{\mathrm{I}}\mathbf{D}$ and $\mathbf{A}$ in model I. Herein, following others,[39,40] we shall take the isotropic part of each ^{29}Si matrix $\mathbf{A}$ to be positive.

The sign choice of matrix $\mathbf{D}$ was selected during the fitting by the signs chosen for the $\mathbf{A}(^{29}\mathrm{Si})$ matrices. This sign appearance is the same as that of matrix $\mathbf{D}$ found for the center $[\mathrm{AlO_4}]^+$ triplet state (oxygenic electron holes).[41]

The six parameters in each matrix $\mathbf{A}$ were calculated to fit corresponding ^{29}Si HF lines. For double-occupancy (^{29}Si) lines, the sum of the two hyperfine terms (α and β) was utilized in the spin Hamiltonian (1).

In all our hyperfine calculations, matrix $\mathbf{g}_n$ was taken to be $g_n\mathbf{E}$, with scalar g_n for ^{29}Si taken from standard tables (Table H.4 of Ref. 34). $\mathbf{E}$ is the 3×3 unit matrix.

As stated, using the natural abundance $100\times\mathrm{NA}=4.69$ at. %, one can estimate the relative intensity (RI) of each member of the ^{29}Si quartet (two lines above the field region of the main lines, and two below) relative to the intensity of either of the main lines (per given site) to be given by $\mathrm{RI} \equiv \mathrm{NA}/[2(1-\mathrm{NA})] = 0.0246$. The observed ratio of RI turned out to be 0.025 ± 0.002. The probability of both sites being simultaneously occupied by ^{29}Si is $(\mathrm{RI})^2 = 0.000\,605$. Such species have, in fact, been observed in our present EPR work (see below, including Fig. 6).

Our results can be discussed using the two models:

(I) Triplet state. Here, we use an effective electron spin, $S=1$. The various parameter matrices $\mathbf{g}$, $^{\mathrm{I}}\mathbf{D}$, $\mathbf{A}(^{29}\mathrm{Si}_\alpha)$, and

TABLE V. Comparison of the ^{29}Si principal hyperfine value data (Tr $\mathbf{A}$ and traceless principal values, in mT) for centers E_1'' (from Table III) and E_1' in α-quartz.

	E_1'' Si_α	E_1'' Si_β	E_1' Expt. [a]	E_1' Theor. [b]
$A_0/(g_e\beta_e)$ $\equiv(1/3)\mathrm{Tr}\,\mathbf{A}/(g_e\beta_e)$ [c]	20.53	19.84	41.150	46.726
$^\circ A_1/(g_e\beta_e)$	2.111	2.156	4.163	4.461
$^\circ A_2/(g_e\beta_e)$	−1.041	−1.071	−2.078	−2.176
$^\circ A_3/(g_e\beta_e)$	−1.070	−1.085	−2.085	−2.283

[a] Reference 9.

[b] Reference 18.

[c] The isotropic component A_0 has been taken to be positive. Hence, $^\circ A_\parallel > 0$ herein, as well as $^\circ A_\parallel - {}^\circ A_\perp > 0$.

TABLE VI. Comparison of the unique directions (site 1) of ^{29}Si hyperfine principal directions for various oxygen-vacancy centers (data from the literature) with the relevant α-quartz structural directions.

		Unique direction		Structural direction [a] (Si-O-Si)		
	Center	θ	φ	θ'	φ'	Reference
E_1'	Si_1	114.1	229.7	113.6	230.7	9
E_1'	Si_1	113	50	113.6	50.7	48 [b]
E_4'	Si_1	103.5	215.8	113.6	230.7	19
	Si_2	42.9	84.4	44	86.3	
E_1''	Si_α	117.8	214.2	113.6	230.7	This study
	Si_β	61.1	84.2	44	86.3	

[a] Cf. Table I.
[b] Left quartz.

$\mathbf{A}(^{29}Si_\beta)$ obtained by best-fitting numerous EPR line positions are given in Tables II and III, along with the principal values and directions associated with them. The lowest root-mean-square deviation (RMSD) obtained is 0.0167 mT for the main lines. We consider that this result is pleasing, in view of the typical linewidths of 0.04 mT encountered. The analogous RMSD values are 0.0341 mT for Si_α and 0.0264 mT for Si_β, higher for reasons to be discussed.

(II) Biradical. An example of biradical energy levels is depicted in Fig. 7. The various parameter matrices $\mathbf{g}_1$, $\mathbf{g}_2$, $^0\mathbf{D}$ as well as the exchange energy $J/g_e\beta_e$, all obtained by best-fitting numerous EPR line positions, are given in Table IV, along with the principal values and directions associated with the matrices. The lowest RMSD obtained for the main-line spectrum is 0.0161 mT, very slightly better than for model I.

Also, in the biradical model, it is expected that matrix $^{II}\mathbf{D}$ be exactly twice matrix $^{I}\mathbf{D}$ of the triplet model (Ref. 6, and p. 163 of Ref. 34). Tables II and IV reveal that this is indeed so. Compare the model-I $\mathbf{D}$ with the model-II $^0\mathbf{D}$. Clearly, deconvolution of the second term in Eq. (3) with the two matrices $\mathbf{g}_i$ is hardly needed, since all g values are so close to g_e. We see (Tables II and IV) that the principal-axis systems of these two matrices $\mathbf{D}$, separately obtained from the same

TABLE VII. The electronic quadrupole parameters D' and point-dipole mean interelectron distances r, estimated from D', for various two-unpaired-electron centers in α-quartz and for gaseous dioxygen. $D' \equiv (D_\parallel - D_\perp)/g_e\beta_e \approx (3/2)\sigma\,(\mu_0/4\pi)g_e\beta_e\langle r^{-3}\rangle = (\sigma/2)5.570\,859\langle r^{-3}\rangle$ [Chap. 6 of Ref. 34]. Here, $\sigma = 1$ for triplet species, and $\sigma = 2$ for biradicals. D' is expressed in mT, and r in nm. Note that D' occurs doubled for biradicals, as compared to D' for triplets.

Type	Species	Model σ	$D' \equiv 3D_z/(2g_e\beta_e)$ [a] (mT)	$r \equiv \langle r^{-3}\rangle^{-1/3}$ (nm)	Reference
Birad	E_1''	1	12.189 [b]	0.611	This study
		2	24.384 [b]		
Birad	E_3''	1	1.33_5	1.277	Unpublished
		2	2.67 [b]		
Birad	X	1	4.66_5	0.842	6
		2	9.33 [b]		
Triplet	$[AlO_4]^+$ [c]	1	35.168 [b]	0.429	41
		2	70.336		
Triplet	O_2 (gas)	1	1871_5	0.114	45 [d]
		2	3743 [b]		

[a] D_z is the largest-magnitude principal value of traceless $\mathbf{D}$, in units of joules.
[b] Reported measured value.
[c] The principal D values for E_1'', using model I, are about three times smaller (Table II) than those of triplet-state center $[AlO_4]^+$ (Ref. 41).
[d] 0.121 nm (experimental).

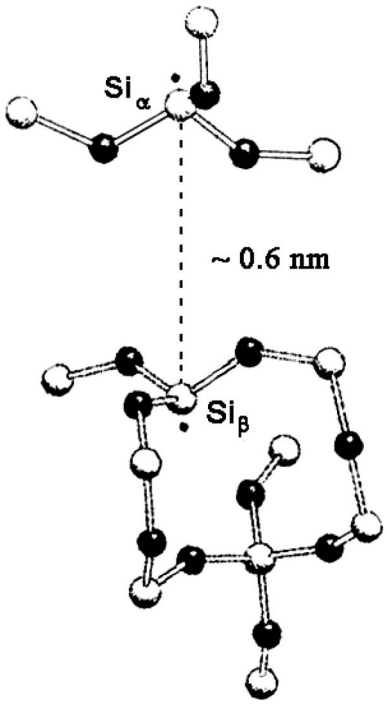

FIG. 8. The proposed model for center E_1''. Figure modified after Lægsgaard (Ref. 33). Note that the two cations Si_α and Si_β (white spheres indicated) are not equivalent: one is attached to the quartz oxygenic structure by two long bonds and one short bond, and the other vice versa. For example, they could represent Si atoms 0 and 1 in Fig. 1.

line-position data, are close to being identical.

Note (Table IV) that matrices $\mathbf{g}_1$ and $\mathbf{g}_2$ are very close to yielding isotropic g values equal to g_e, i.e., that ${}^{\mathrm{II}}\mathbf{D} \sim {}^{0}\mathbf{D}$ [Eq. (3)] and, thus, is virtually traceless. Although the g values are almost isotropic, the anisotropy and measuring accuracy for the main-line spectra are sufficient to yield a matrix $\mathbf{g}$ which turns out to be closely coaxial with $\mathbf{D}$ (Table II), i.e., this demonstrates that $\mathbf{g}$ for triplet E_1'' has been accurately determined. Comparing with model II (Table IV), we note that $\mathbf{g}_1$ and $\mathbf{g}_2$ here are not quite as accurate, but that their average comes very close to being equal to $\mathbf{g}$ of model I. We note that all three matrices $\mathbf{g}$ deviate somewhat from being exactly uniaxial. The unique axes of $\mathbf{g}_1$ and $\mathbf{g}_2$ differ considerably from being close to the Si-Si direction (Tables I and IV).

The energy spacing between the singlet and triplet states of a two-unpaired-electron system is generally considered hardly to affect the EPR line positions. On the other hand, intensity (state population) measurements at the appropriate temperatures can readily give relevant information about the relative spacing.

However, we realize that the energy spacing of the two manifolds does affect the line positions in some circumstances. In particular, when the matrices $\mathbf{g}$ of the two electrons are not identical, then EPR transitions between triplet levels and the singlet do become somewhat allowed. This effect does not depend on the anisotropy of either $\mathbf{g}$ or on whether $\mathbf{D}$ has a nonzero trace, i.e., on whether J is zero. Also, taking the signs of the two matrices $\mathbf{g}$ to be opposite shows no effect. The dependence of the spin energy levels, transition frequencies, and positions has been calculated by perturbation theory and their dependences on J explicitly shown.[42] Also, see Ref. 43. In our work, the value of J turns out to be not unique. For instance, we obtained almost equally good fittings with the values $J/(g_e\beta_e) = -6.8 \pm 1.8$ mT and $J/(g_e\beta_e) = +59 \pm 28$ mT. Thus, all we can say is that J appears to be of the same magnitude as D_Z, with the singlet state lying near in energy to the central level of the triplet (Fig. 7). However, as we see, the values of J are error prone, consistent with our expectations and with expressed ideas (Sec. 9.5 of Ref. 44).

V. DISCUSSION

The parameter matrices presented in Tables II–IV suffice to construct a model of E_1''. The main idea is to postulate that a single oxygen vacancy is present, of the form $V(\mathrm{O})^0$. This breaks the local symmetry at the two adjacent Si cations to being merely C_1, as is observed. The silicon atoms on opposite sides of V each carry an electron hole, so that the center is a biradical. One aspect is that we find that E_1'' has its spin singlet sufficiently close energetically to its triplet manifold that it better not be ignored.

The spin Hamiltonians (1) and (2) both utilized gave fine fits to the crystal-rotational EPR data, with the latter very slightly better. It, of course, features seven additional parameters to be fitted (see Tables II and IV). We note happily that the matrices $\mathbf{D}$ in both cases are close to being uniaxial, with the same unique axis. For the crystal site labeled 1 by us (Tables II and IV), the unique D axis occurs at (θ, ϕ) orientation 56.0°, 56.5° which is close (about 10°) to the Si0-Si1 direction 53.9°, 66° (Table I). Thus, we can establish a reasonable link between the spin-Hamiltonian parameter directions and the quartz atomic structure. Once the correct choice of site (among the six) is at hand for one parameter matrix (i.e., $\mathbf{D}$), this is valid for all the parameter matrices.

One can note that the parameter matrices $\mathbf{g}_1$ and $\mathbf{g}_2$ are inequivalent (Table IV), i.e., have appreciably different principal values. Thus, the two spin members of the biradical are not equivalent, differing slightly in their physical properties. The middle principal values and axes seem to coincide. However, the principal-axis systems are "inverted," with the same angle sets but with the largest principal g values exchanged for the smallest in comparing $\mathbf{g}_1$ and $\mathbf{g}_2$. In other words, a rotation by 90° about the middle-value shared axis tends to interchange the two matrices.

The ^{29}Si hyperfine matrices for the two distinctly different Si sites, obtained with model I, are presented in Table III. These two matrices $\mathbf{A}$ are very similar, and are not far from uniaxial. The unique axis directions of the two $\mathbf{A}(^{29}\mathrm{Si})$ matrices fitted in model I are almost coaxial, the angular deviation between them being 4.4°.

In Fig. 6, we display the expected EPR spectrum for E_1'' when both its Si sites are occupied by ^{29}Si. Clearly, it is quite a complex one. We have successfully observed several of these lines (very weak) in the c-axis RT spectrum. The observed relative intensity of these lines compared to the singly occupied hyperfine lines appears consistent with the probability of both sites being simultaneously occupied by ^{29}Si,

i.e., $(RI)^2 = 6.05 \times 10^{-4}$, about 1/40 the concentration of the singly occupied site. In the region of interest, many weak lines from other centers are also seen.

Table V features a comparison of our ^{29}Si hyperfine data, principal values, with those of E_1', both experimental and theoretical values for the latter. We note that there is considerable resemblance between the two centers, with the isotropic hyperfine components of E_1' roughly double those of E_1''. The traceless hyperfine matrices for all are close to uniaxial, with E_1'' showing a relatively smaller rhombic component. Also included, in Table VI, is a comparison of the ^{29}Si unique directions with quartz structural directions for E_1'' and centers E_1' and E_4'.

We have compared matrix **D** obtained (main lines) in the absence of **A**(^{29}Si) (Table II) with the matrix **D** obtained when optimizing the data with a HF matrix included. We found the latter to be virtually the same but somewhat less accurate, since the ^{29}Si spectra are weak and complex.

Since **D** is very close to being uniaxial (Table II), one can attempt to interpret the principal values assuming the simple point magnetic dipole-dipole theory. This yields an estimated interspin distance of 0.61 nm (Table VII). The smallest Si-Si distance of pure quartz is 0.3 nm (Table I and Figs. 1 and 8). Thus, within the oxygen-vacancy model, we visualize the two spin-bearing silicon anions as retreating from each other. For some measure of the validity of the point-dipole model for **D**, we cite our result (Table VII) for the well-characterized triplet molecule O_2.[45]

Attempts to vary the ^{29}Si matrices $\mathbf{g}_n$ did not yield any meaningful improvements in the line-position fittings. Thus, these matrices were kept "isotropic" in all computations.

VI. CONCLUSIONS

Single-crystal rotation studies by EPR spectroscopy have yielded accurate spin-Hamiltonian parameters for the center called E_1'', created by radiation-damage processes in α-quartz. It is concluded that this center contains two unpaired electrons, and is somewhat better described as a biradical species rather than as a triplet-state species. Perhaps the most important aspect of this is that, with the latter model, we can extract a meaningful pair of **g** matrices which are slightly different, mirroring distinct aspects of the two spin sites.

Analysis suggests that E_1'' features an oxygen (O^0) vacancy, with the unpaired electrons existing at opposite ends of the cavity on silicon cations. The exchange interaction is roughly of the same magnitude as the magnetic dipolar interaction between them, so that the biradical model is more appropriate.

With regards to future considerations, little is known as yet about the temperature dependence of the spin-Hamiltonian parameters or the thermal dependence of the state populations. Unfortunately also, almost nothing is yet understood about the radiation physics behind the various E' and E'' centers. Work in these areas is needed. We hope to present accurate data for another biradical species found in α-quartz, e.g., E_3'', mentioned earlier in this paper. Hopefully, it will soon become clear why there should exist a whole family of E'' centers and how they are interrelated.

Obviously also, the time has come for serious quantum-mechanical modeling of center E_1''.

ACKNOWLEDGMENTS

R.I.M. acknowledges support from the Russian Foundation for Basic Research (Grant No. 07-05-00022). This research was also supported in part by the Natural Sciences and Engineering Research Council (NSERC) of Canada, and in part by one of the authors (J.A.W.).

*rim@uiggm.nsc.ru
†john.weil@usask.ca

[1] D. Rugar, R. Budakian, H. J. Mamin, and B. W. Chui, Nature (London) **430**, 329 (2004).
[2] J. A. Weil, Phys. Chem. Miner. **10**, 149 (1984).
[3] J. A. Weil, in *The Physics and Chemistry of* SiO_2 *and the* Si-SiO_2 *Interface*, edited by C. R. Helms and B. E. Deal (Pergamon, New York, 1993), Vol. 2, p. 131.
[4] J. A. Weil, in *Defects in* SiO_2 *and Related Dielectrics: Science and Technology*, edited by G. Pacchioni *et al.* (Kluwer Academic, Dordrecht, 2000), p. 197.
[5] M. Boero, A. Oshiyama, and P. L. Silvestrelli, Mod. Phys. Lett. B **18**, 707 (2004).
[6] J. Isoya, W. C. Tennant, Y. Uchida, and J. A. Weil, J. Magn. Reson. **49**, 489 (1982).
[7] R. A. Weeks and C. M. Nelson, J. Am. Ceram. Soc. **43**, 399 (1960).
[8] R. H. Silsbee, J. Appl. Phys. **32**, 1459 (1961).
[9] M. G. Jani, R. B. Bossoli, and L. E. Halliburton, Phys. Rev. B **27**, 2285 (1983).
[10] F. J. Feigl, W. B. Fowler, and K. L. Yip, Solid State Commun. **14**, 225 (1974).
[11] J. K. Rudra and W. B. Fowler, Phys. Rev. B **35**, 8223 (1987).
[12] D. C. Allan and M. P. Teter, J. Am. Ceram. Soc. **73**, 3247 (1990).
[13] K. C. Snyder and W. B. Fowler, Phys. Rev. B **48**, 13238 (1993).
[14] M. Boero, A. Pasquarello, J. Sarnthein, and R. Car, Phys. Rev. Lett. **78**, 887 (1997).
[15] T. Uchino and T. Yoko, Phys. Rev. B **74**, 125203 (2006).
[16] Z. Y. Lu, C. J. Nicklaw, D. M. Fleetwood, R. D. Schrimpf, and S. T. Pantelides, Phys. Rev. Lett. **89**, 285505 (2002).
[17] D. J. Chadi, Appl. Phys. Lett. **83**, 437 (2003).
[18] M. Boero, A. Oshiyama, and P. L. Silvestrelli, Phys. Rev. Lett. **91**, 206401 (2003).
[19] J. Isoya, J. A. Weil, and L. E. Halliburton, J. Chem. Phys. **74**, 5436 (1981).
[20] P. E. Blöchl, Phys. Rev. B **62**, 6158 (2000).
[21] A. S. Mysovsky, P. V. Sushko, S. Mukhopadhyay, A. H. Edwards, and A. L. Shluger, Phys. Rev. B **69**, 085202 (2004).
[22] S. Mukhopadhyay, P. V. Sushko, A. M. Stoneham, and A. L. Shluger, Phys. Rev. B **70**, 195203 (2004).

[23] R. A. Weeks, Phys. Rev. **130**, 570 (1963).
[24] J. K. Rudra, W. B. Fowler, and F. J. Feigl, Phys. Rev. Lett. **55**, 2614 (1985).
[25] B. D. Perlson and J. A. Weil (unpublished).
[26] R. A. Weeks and M. M. Abraham, Bull. Am. Phys. Soc. **10**, 374 (1965).
[27] V. P. Solntsev, R. I. Mashkovtsev, and M. Ya. Shcherbakova, J. Struct. Chem. **18**, 578 (1977).
[28] R. B. Bossoli, M. G. Jani, and L. E. Halliburton, Solid State Commun. **44**, 213 (1982).
[29] G. Buscarino, S. Agnello, and F. M. Gelardi, Phys. Rev. B **73**, 045208 (2006).
[30] D. L. Griscom and E. J. Friebele, Phys. Rev. B **34**, 7524 (1986).
[31] R. Tohmon, Y. Shimogaichi, Y. Tsuta, S. Munekuni, Y. Ohki, Y. Hama, and K. Nagasawa, Phys. Rev. B **41**, 7258 (1990).
[32] S. P. Karna, A. C. Pineda, W. M. Shedd, and B. K. Singaraju, in *Proceedings on Silicon-on-Insulator Technology and Devices*, edited by P. L. F. Hemment (Electrochemical Society, Pennington, NJ, 1999), Vol. 99-3, pp. 161–166.
[33] J. Lægsgaard, Phys. Rev. B **66**, 024107 (2002).
[34] J. A. Weil and J. R. Bolton, *Electron Paramagnetic Resonance*, 2nd ed. (Wiley, New York, 2007).
[35] Y. Le Page, L. D. Calvert, and E. J. Gabe, J. Phys. Chem. Solids **41**, 721 (1980).
[36] R. H. D. Nuttall and J. A. Weil, Can. J. Phys. **59**, 1696 (1981).
[37] J. A. Weil, T. Buch, and J. E. Clapp, Adv. Magn. Reson. **6**, 183 (1973).
[38] M. J. Mombourquette and J. A. Weil, EPR-NMR, Version 6.5.3, Department of Chemistry, University of Saskatchewan, 2007.
[39] A. Stirling and A. Pasquarello, J. Phys.: Condens. Matter **17**, S2099 (2005).
[40] M. Sprenger, S. H. Muller, E. G. Sieverts, and C. A. J. Ammerlaan, Phys. Rev. B **35**, 1566 (1987).
[41] R. H. D. Nuttall and J. A. Weil, Can. J. Phys. **59**, 1886 (1981).
[42] V. N. Parmon, A. I. Kokorin, and G. M. Zhidomirov, J. Magn. Reson. (1969-1992) **28**, 339 (1977).
[43] K. Itoh, H. Hayashi, and S. Nagakura, Mol. Phys. **17**, 561 (1969).
[44] A. Abragam and B. Bleaney, *Electron Paramagnetic Resonance of Transition Ions* (Clarendon, Oxford, 1970).
[45] For a comparison, we can invoke dioxygen in its ground (triplet) state: $d_{\mathrm{O\text{-}O}}=0.121$ nm; $D/g_e\beta_e=+3743$ mT (Ref. 46), with its singlet state occurring much higher, by about 10^7 mT. See the entry in Table VII. We also note that **g** for E_1'' is not far from matching matrix **g** for dioxygen (Ref. 47).
[46] E. van der Horst and P. J. M. van Bentum, Physica B **294-295**, 87 (2001).
[47] N. Bjerre, J. Chem. Phys. **76**, 3347 (1982).
[48] F. J. Feigl and J. H. Anderson, J. Phys. Chem. Solids **31**, 575 (1970).